Supplement of

Historical (1960–2014) lightning and LNO_x trends and their controlling factors in a chemistry–climate model

Yanfeng He et al.

Correspondence to: Yanfeng He (hyf412694462@gmail.com)

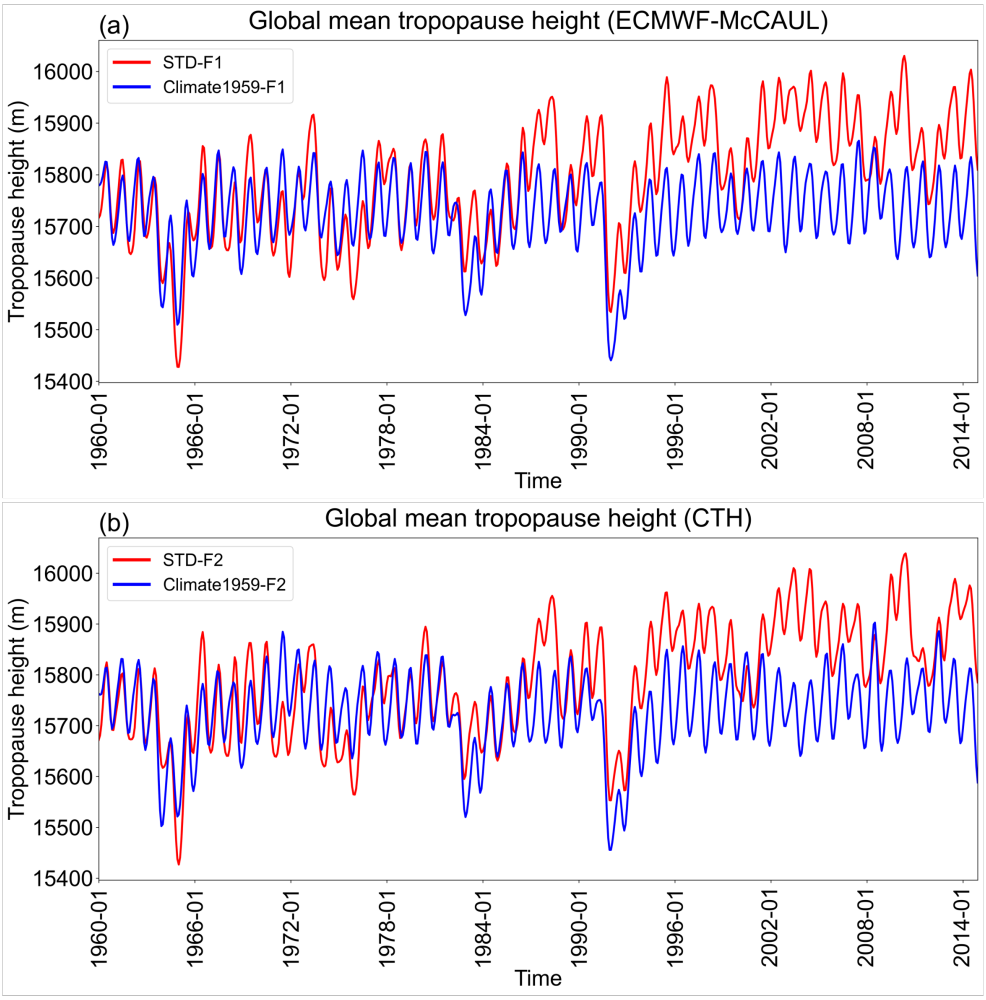

Figure S1: Monthly time-series data of global mean tropopause height with a 1-D Gaussian (Denoising) Filter applied simulated by the ECMWF-McCAUL scheme (a) and the CTH scheme (b).

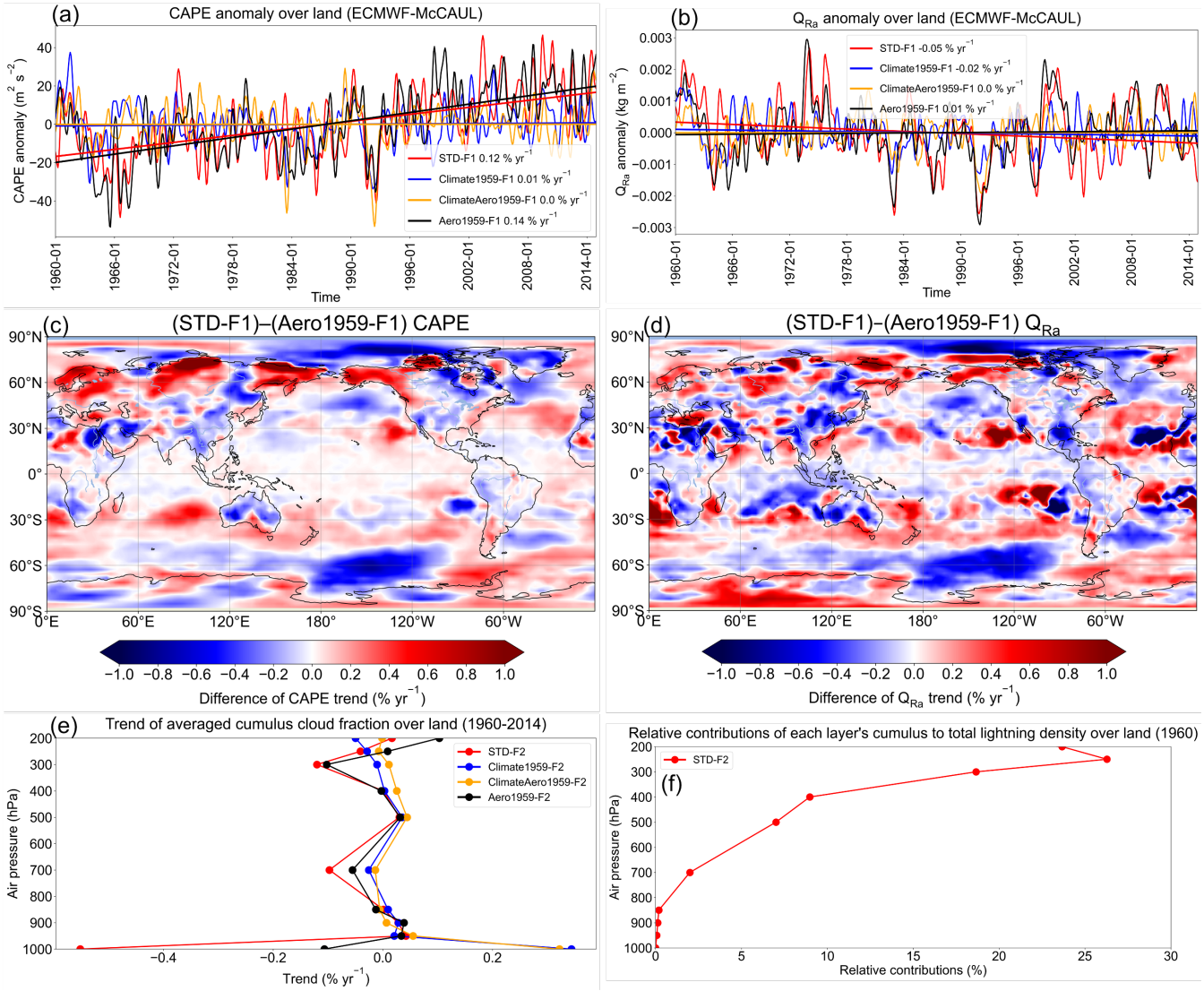

Figure S2: Figures S2 (a) and (b) respectively show monthly time-series data of terrestrial average CAPE and Q_{Ra} anomalies with 1-D Gaussian (Denoising) Filter applied and their fitting curves simulated by the ECMWF-McCAUL scheme. Figures S2(c) and S2(d) respectively show the difference in the CAPE trend and Q_{Ra} trend of the STD-F1 and Aero1959-F1 experiments in the global map. Figure S2e shows the vertical profiles of the terrestrial average cumulus cloud fraction trend simulated by the CTH scheme. Figure S2f shows the relative contributions of each layer's cumulus to total lightning density over land regions in 1960, as calculated from the outputs of the STD-F2 experiment.

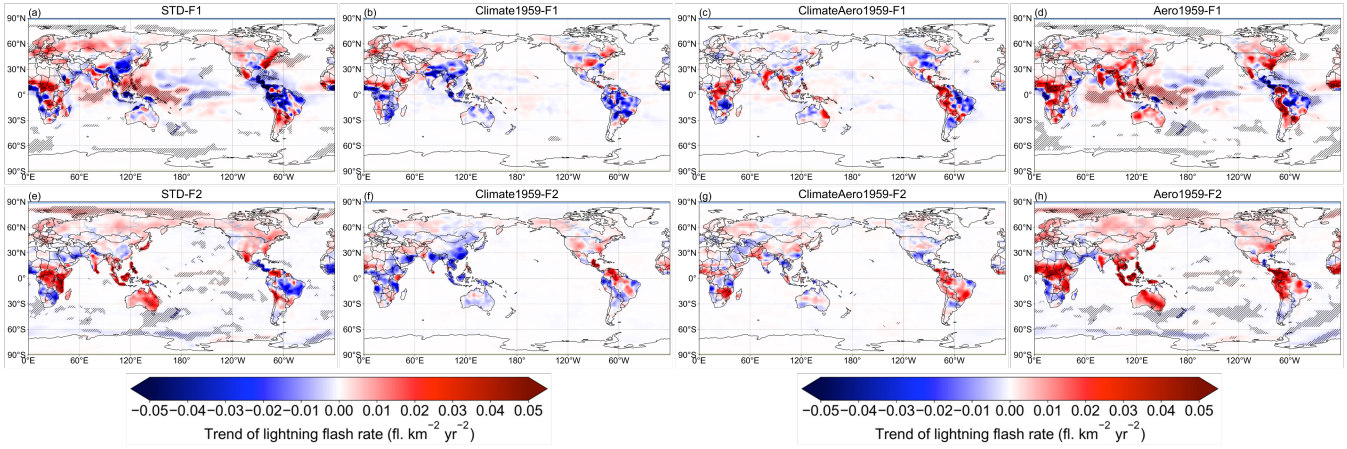

Figure S3: Lightning flash rate trends (fl. km^{-2} yr^{-2}) during 1960–2014 on the two-dimensional map. The trend at every point was calculated from the function of approximating curve for the 1960–2014 time-series data at each grid cell. The area in which the trend was found to be significant by the Mann–Kendall rank statistic test (significance level inferred for 5%) is marked with hatched lines.

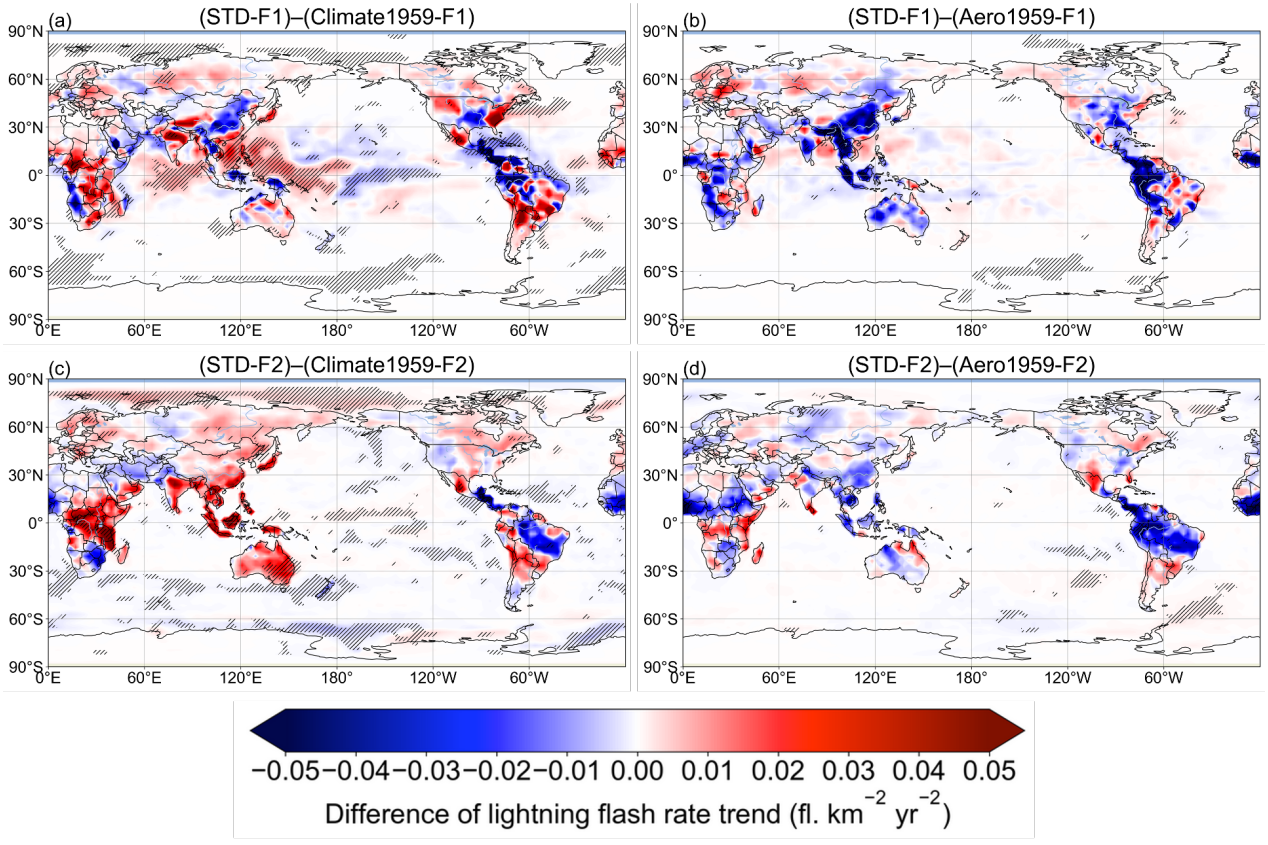

Figure S4: Differences in lightning flash rate trends (fl. km^{-2} yr^{-2}) during 1960–2014 on the global map. The area in which the trend of the differences of lightning flash rate time-series data was found to be significant by the Mann–Kendall rank statistic test (significance level inferred for 5%) is displayed with hatched lines.

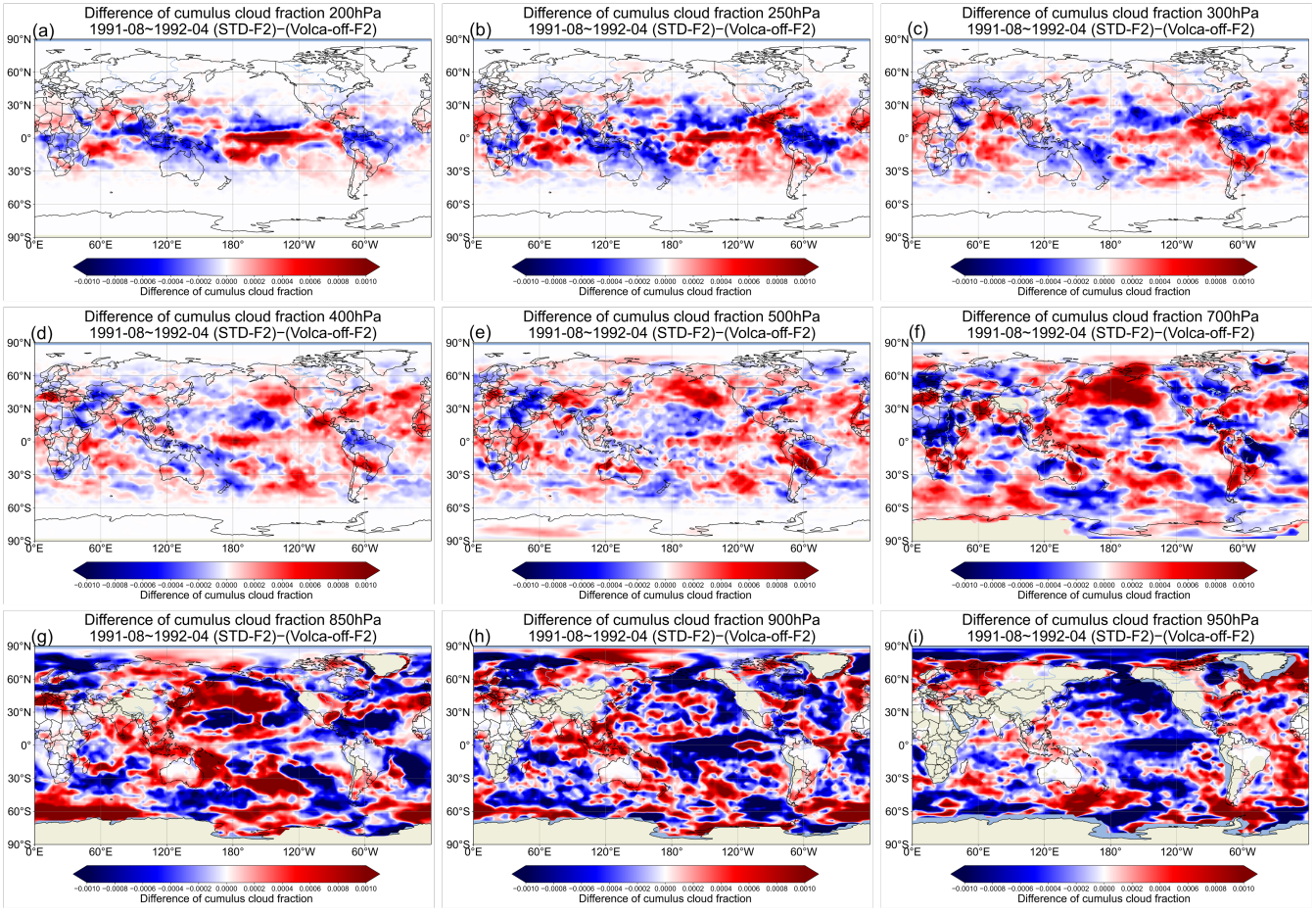

Figure S5: 1991-08 – 1992-04 averaged differences of cumulus cloud fractions at different pressure levels between STD-F2 and Volca-off-F2 experiments on the global map.

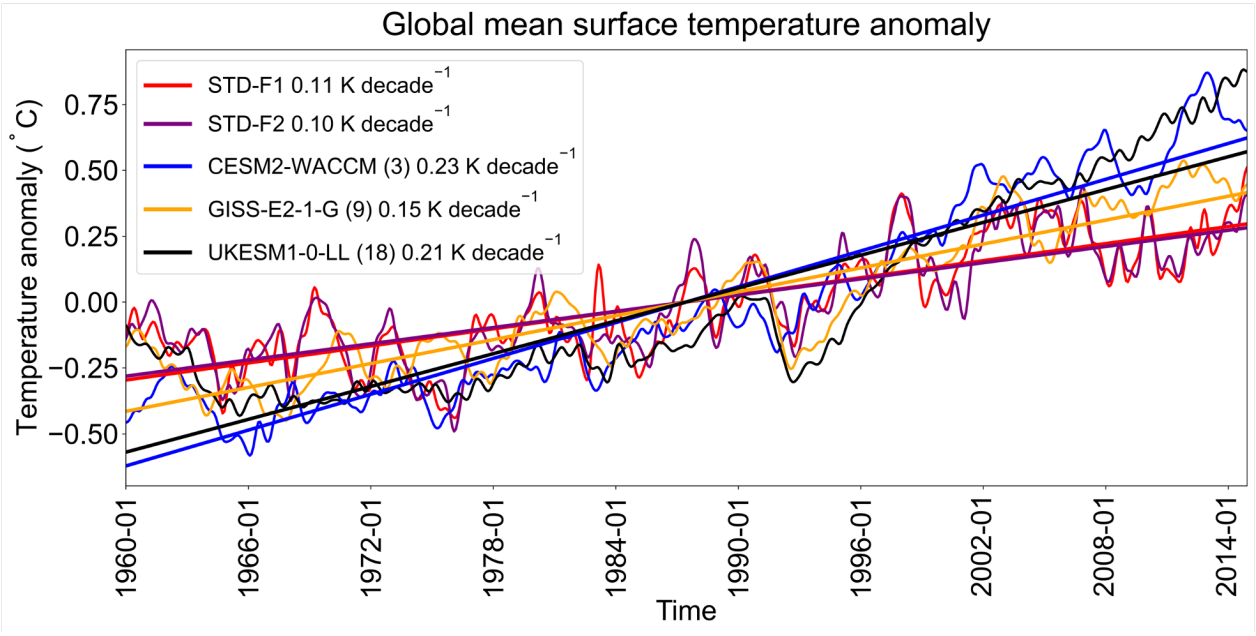

Figure S6: Simulated global mean surface temperature anomalies of our study (CHASER) compared with other CMIP6 models. This figure was created based on the monthly time-series data of global mean surface temperature anomalies with 1-D Gaussian (Denoising) Filter applied. For CMIP6 models, the ensemble mean is shown by the solid line. The fitting curves and the trends of fitting curves (K decade^{-1}) are also presented in this figure.

Table S1: All the ensemble members (displayed as variant labels) used for this study

CESM2-WACCM (3 ensembles)	GISS-E2-1-G (9 ensembles)	UKESM1-0-LL (18 ensembles)
r1i1p1f1	r1i1p3f1	r1i1p1f2
r2i1p1f1	r1i1p5f1	r2i1p1f2
r3i1p1f1	r2i1p5f1	r3i1p1f2
	r3i1p3f1	r4i1p1f2
	r3i1p5f1	r5i1p1f3
	r4i1p3f1	r6i1p1f3
	r4i1p5f1	r7i1p1f3
	r10i1p3f1	r8i1p1f2
	r10i1p5f1	r9i1p1f2
		r10i1p1f2
		r11i1p1f2
		r12i1p1f2
		r14i1p1f2
		r15i1p1f2
		r16i1p1f2
		r17i1p1f2
		r18i1p1f2
		r19i1p1f2